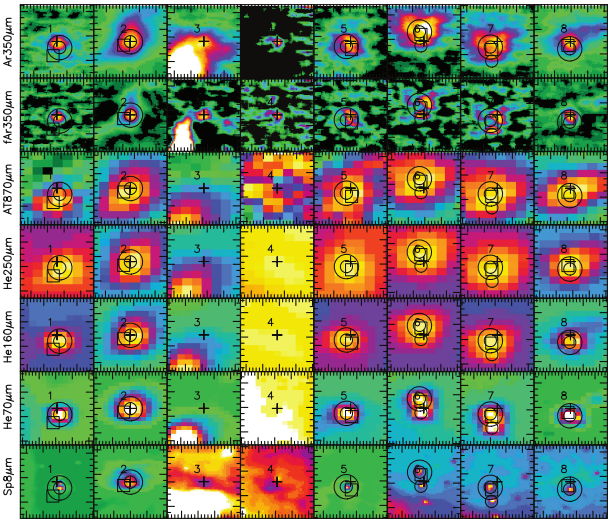

Figure C24. Same as Fig. C1 but for the SDC343 field.

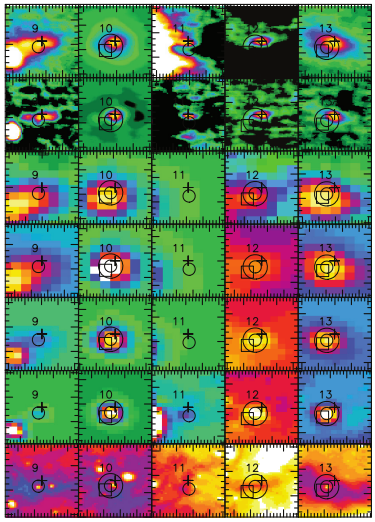

Figure C25. Fig. C20 continued.

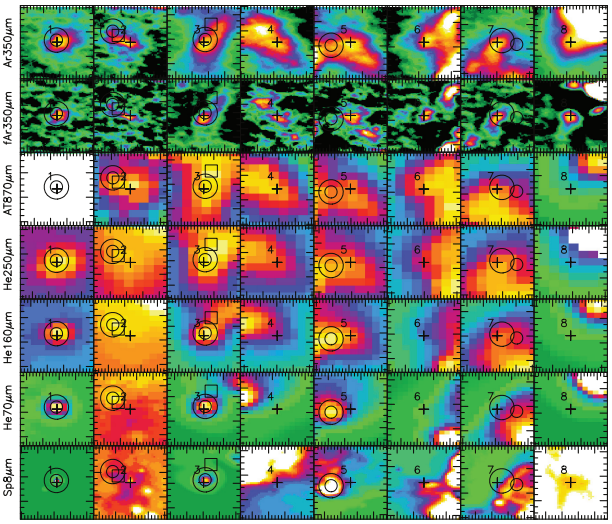

Figure C26. Same as Fig. C1 but for the SDC345 field.

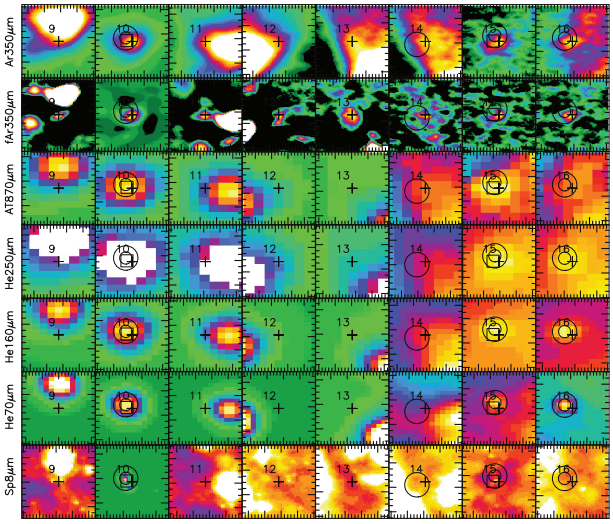

Figure C27. Fig. C22 continued.

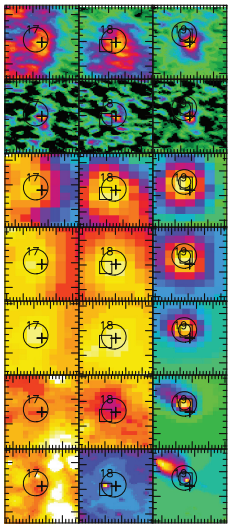

Figure C28. Fig. C22 continued.

APPENDIX D: ALTERNATIVE DUST TEMPERATURE ASSUMPTION

As mentioned in Section 6, *all* core temperatures displayed in Fig. 5 are derived from equation (5). This relationship has been partly inferred from the observed correlation between the internal temperature and the colour temperature of protostellar sources (see Fig. 4). The choice of applying equation (5) to both protostellar and starless sources is justified by the absence of correlation between the ratio $\overline{T}_{\rm int}/T_{\rm col}$ and the source internal luminosity. However, for completeness, we here show the mass versus temperature diagram where the dust temperatures of starless sources are estimated using $T_{\rm dust} = T_{\rm col}$ while using $T_{\rm dust} = 1.2 \times 1.32 \times T_{\rm col}$ for protostellar sources (as in Fig. 6). The 1.2 factor is taken from equation (5), while the 1.32 factor corresponds to the rescaling from 0.23 pc (the original resolution of the temperature data) to 0.1pc (see Section 6). The resulting mass versus temperature diagram is shown in Fig. D1.

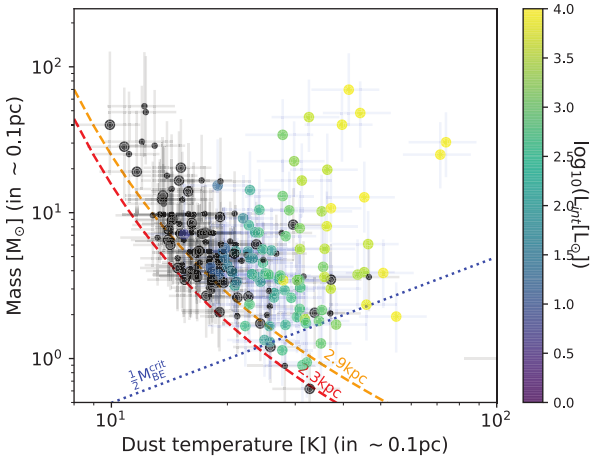

Figure D1. Same as Fig. 6 but with starless source's temperatures estimated using $T_{\rm dust} = T_{\rm col}$ as opposed to $T_{\rm dust} = 1.2T_{\rm col}$.

APPENDIX E: MODELS WITH $R_{\rm CORE}$ = 1000 AU

Fragmentation on scales of a couple of thousands AU scale (e.g. Bontemps et al. 2010; Motte et al. 2018a; Beuther et al. 2018), or even smaller scale (e.g. Palau et al. 2013), is routinely observed in massive star-forming regions. In an attempt to produce similar model/data comparisons as those presented in Figs 7 and 8 but at a core scale of 0.01pc (i.e. $R_{\rm core}$ = 1000 AU), we rescaled the data as follows. For all sources, we assumed a density profile scaling as $\rho \propto r^{-2}$, which in practice implies a decrease of the core masses by a factor of 10 compared to the $R_{\rm core}$ = 0.05 pc case. Regarding the temperatures of protostellar sources, we used equation (1) with the relevant radius, which in practice means an increase of the temperature by a factor of 2.1 compared to the $R_{\rm core}$ = 0.05 pc case. Finally, we leave unchanged the temperatures of starless sources. We here keep the same fractional temperature uncertainties of 20 per cent; however, these are most likely much larger. The resulting observed core temperatures and masses are displayed as grey symbols in Figs E1 and E2.

Fig. E1 shows a set of core-fed models, with six different initial cores masses, $m_{\rm core}(t = 0)$ = [0.5, 1, 2, 4, 8, 16] M$_\odot$. We kept the time-scale $\tau_{\rm core}$ the same as in the $R_{\rm core}$ = 0.05 pc but increased the core to star formation efficiency to $\epsilon_{\rm cs} = 1$, the maximum allowed for core-fed models. Unsurprisingly, the conclusions here are similar to those drawn from the $R_{\rm core}$ = 0.05 pc models, which is that they fail to explain the formation of the most massive stars (no massive pre-stellar cores) but may be compatible with the formation of intermediate-mass stars. The fact that one needs to use $\epsilon_{\rm cs} = 1$ to get a reasonable match with the data does show that massive star-forming cores on these sort of scales do need to accrete mass from radii that are larger than the last fragmentation scale. This is somewhat explicit, given the low core masses.

Fig. E2, on the other hand, shows clump-fed tracks with an initial core mass $m_{\rm core}(t = 0) = 0.1$ M$_\odot$, a core formation efficiency $\epsilon_{\rm cc}$ = 0.01, and a core to star formation efficiency $\epsilon_{\rm cs} = 1$. Clump masses are identical to those used for the $R_{\rm core}$ = 0.05 pc models. Here again, as far as the most massive objects are concerned, we see that the clump-fed models are in better agreement with the observations. And similarly to the core-fed models, the use of $\epsilon_{\rm cs} = 1$ shows that larger scale accretion is required.

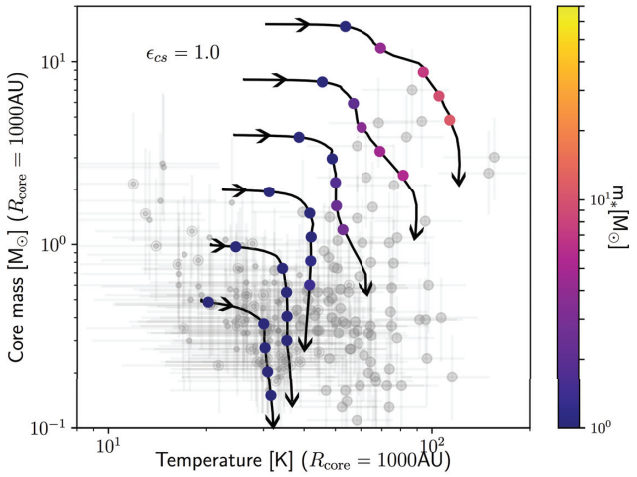

Figure E1. Core-fed models. Each track has been computed for a different initial core mass, from bottom to top $m_{\rm core}(t = 0)$ = [0.5, 1, 2, 4, 8, 16] M$_\odot$. The coloured symbols represent the position of the cores at times t = [9 × 10^3, 9 × 10^4, 1.8 × 10^5, 2.7 × 10^5, 3.6 × 10^5] yr. The colour codes the stellar mass at these times as displayed by the colour bar. The background grey symbols are the ArTéMiS sources whose properties have been rescaled to 0.01pc (see text). Note that sources with $M_{\rm gas} < \frac{1}{2}M_{\rm BE}^{\rm crit}$ have been removed.

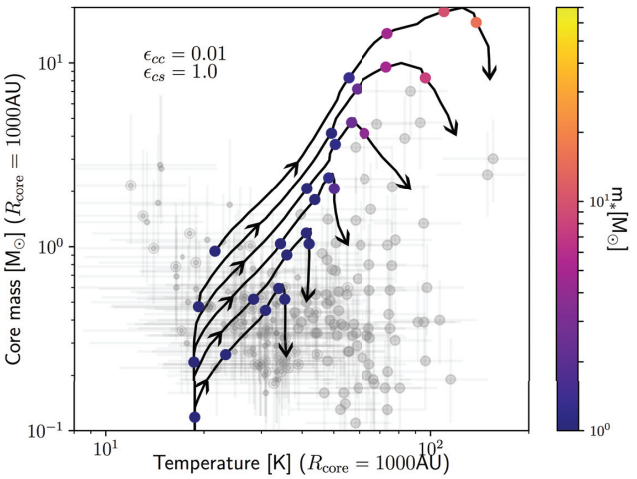

Figure E2. Clump-fed models. Each track has been computed for a different clump mass, from bottom to top $m_{\rm clump}$ = [100, 200, 400, 800, 1600, 3200] M$_\odot$.The coloured symbols represent the position of the cores at times t = [3 × 10^4, 3 × 10^5, 6 × 10^5, 9 × 10^5, 1.2 × 10^6] yr. The colour codes the stellar mass at these times as displayed by the colour bar. The background grey symbols are those presented in Fig. E1. Note that sources with $M_{\rm gas} < \frac{1}{2}M_{\rm BE}^{\rm crit}$ have been removed.

This paper has been typeset from a TEX/LATEX file prepared by the author.